# Graphical abstract

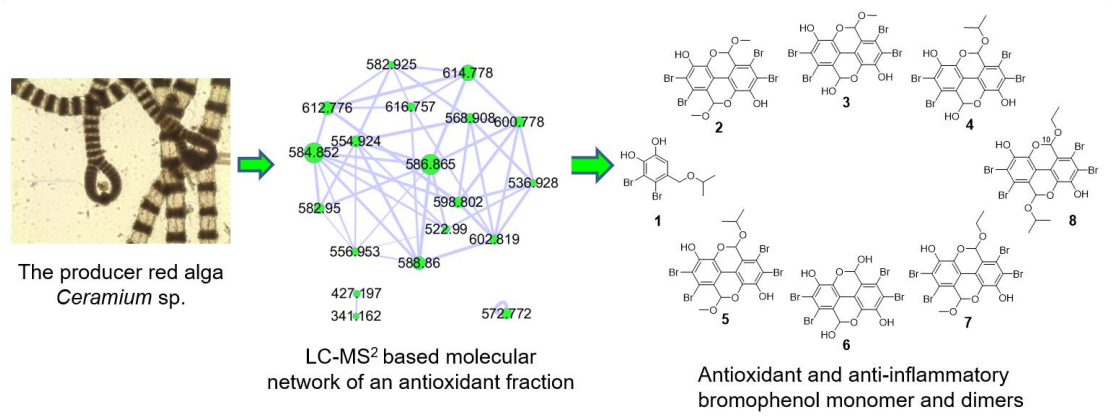

# Monomeric and dimeric bromophenols from the red alga *Ceramium* sp. with antioxidant and anti-inflammatory activities

Yi Zhang[a,b,c,d], Evgenia Glukhov[c], Haobin Yu[c], Lena Gerwick[c], Pieter C. Dorrestein[e], William H. Gerwick[ce*]

[a] *College of Food Science and Technology, Guangdong Provincial Key Laboratory of Aquatic Product Processing and Safety, Guangdong Province Engineering Laboratory for Marine Biological Products, Research Institute for Marine Drugs and Nutrition, Guangdong Ocean University, Zhanjiang, 524088, China*

[b] *Shenzhen Institute of Guangdong Ocean University, Shenzhen, 518120, China*

[c] *Center for Marine Biotechnology and Biomedicine, Scripps Institution of Oceanography, University of California, San Diego, La Jolla, California, 92093, United States*

[d] *Collaborative Innovation Center of Seafood Deep Processing, Dalian Polytechnic University, Dalian, 116034, China*

[e] *Skaggs School of Pharmacy and Pharmaceutical Sciences, University of California, San Diego, La Jolla, California, 92093, United States*

[*] Corresponding author: E-mail addresses: wgerwick@ucsd.edu. (W. H. Gerwick)

Abstract

LC-$MS^2$-based molecular networking using the Global Natural Products Social (GNPS) tool revealed a rich assortment of brominated compounds present in the antioxidant fraction of a red algal extract (*Ceramium* sp.) Further chemical investigation led to discovery of one monomeric bromophenol (lanosol isopropyl ether, **1**) and seven dimeric ones (bromourceolatols A−G, **2**−**8**), all of which are previously undescribed. Their structures were elucidated by extensive analysis of their spectroscopic data. Compounds **2**−**8** were determined to be racemic trans-type isomers by NOESY, specific optical rotation, and ECD. Compounds **1** and **3** displayed antioxidant activity with their $EC_{50}$ of 44.4 and 47.0 μM, respectively, for scavenging DPPH free radicals while compounds **2** and **4** had approximate $EC_{50}$ values of ~ 64 μM. Furthermore, compounds **2**, **3**, and **7** exhibited relatively potent anti-inflammatory activity at 32 μM by quenching 97%, 47%, and 73% of nitric oxide induced by bacterial lipopolysaccharide in macrophage RAW264.7 cells, respectively.

Keywords: *Ceramium* sp., bromophenols, antioxidant, anti-inflammatory

## 1. Introduction

Oxidative stress, chronic inflammation and their complex interactions are well recognized to commonly be involved in the etiology of various diseases including cancer, age-related diseases such as Alzheimer's disease and Parkinson's disease, metabolic disorders like obesity, diabetes and cardiovascular diseases, as well as others (Alfadda and Sallam, 2012; Franceschi and Campisi, 2014; Leszek et al., 2016; McBean et al., 2017; Rani et al., 2016; Reuter et al., 2010; Siti et al., 2015). Use of anti-oxidative and anti-inflammatory natural products has been suggested as a possible preventive and therapeutic approach to treat these challenging health conditions, as revealed by numerous preclinical, clinical and epidemiological studies (Alfadda and Sallam, 2012; McBean et al., 2017; Rani et al., 2016; Spagnuolo et al., 2018). Thus, seeking more effective antioxidant and anti-inflammatory natural products is an important medicinal goal.

Seaweeds are renewable and thus are valuable sources of naturally occurring antioxidants and anti-inflammatory agents (Lee et al., 2013). They are able to produce diverse types of natural products, including phenols, sulphated polysaccharides, alkaloids, terpenoids, fatty acids and lipid derivatives, proteins, peptides, amino acids, and others, of which quite a few show both antioxidant and anti-inflammatory activities (Fernando et al., 2016; Wang et al., 2014). Among them, bromophenols are mainly produced by red alga and thus represent a unique family of metabolites. From red alga belonging to the family Rhodomelaceae (in the order of Ceramiales), e.g. genera of *Rhodomela*, *Symphyocladia*, *Polysiphonia*, *Vetebrata*, and *Odonthalia*, a number of

antioxidant and anti-inflammatory bromophenols have been reported (Choi et al., 2018; Gribble, 2015; Jesus et al., 2019; Nogueira et al., 2014; Wang et al., 2013; Wiemer et al., 1991). However, the genus *Ceramium* which is in the family Ceramiaceae (Ceramiales), has only been investigated cursorily for its natural products. One previous investigation of *C. tenuicorne* from the Baltic Sea revealed the presence of known brominated diphenyl ethers by GC-MS analysis (Dalgren et al., 2015) whereas another early study of *C. washingtoniense* from British Columbia was reported to contain one known bromophenol (2,3-dibromo-4,5-dihydroxybenzyl alcohol, lanosol) (Phillips; and Towers, 1981). The former of these were proposed to act as $H_2O_2$ scavengers during photosynthesis, or to be involved in chemical signaling or chemical defense of the seaweed (Dahlgren et al., 2015; Dahlgren et al., 2016; Lindqvist et al., 2017; Malmvarn et al., 2005). However, to date no new bromophenols have been isolated from this genus, and none have been evaluated for their antioxidant or anti-inflammatory activities.

An anti-oxidant assay was run for a 2,800 member library of marine macroalgal and cyanobacterial extracts, and resulted in identifying a fraction of the red alga *Ceramium* sp. as displaying potent 2,2-diphenyl-1-picrylhydrazyl (DPPH) free radical scavenging activity. LC-MS and Global Natural Products Social Molecular Networking (GNPS) (Wang et al., 2016) analysis disclosed the presence of a series of structurally related brominated compounds in this sample. Further HPLC separation, structural analysis by NMR, MS and UV, and anti-inflammatory and antioxidant testing led to the discovery of eight new metabolites, comprised of one monomeric (lanosol isopropyl ether, **1**) and

seven dimeric bromophenols (bromourceolatols A−G, **2**−**8**) (Fig. 1). Herein, we report on their isolation, structure elucidation, and biological properties.

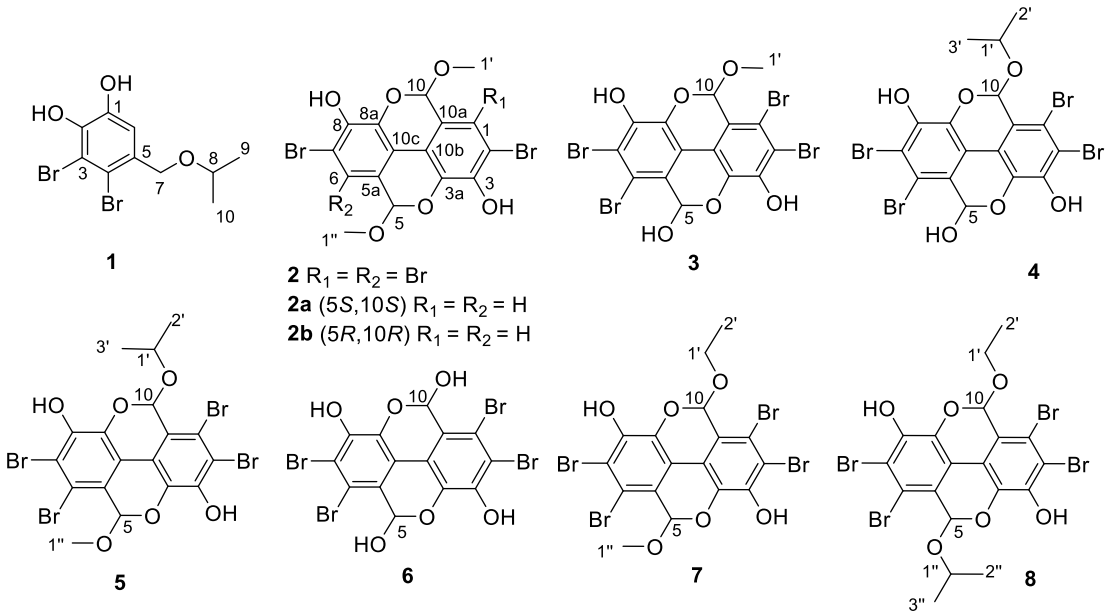


**Fig**. **1**. The structures of compounds **1**−**8** and two reference compounds **2a** and **2b**.

## 2. Results and Discussion

### *2.1 Discovery of Ceramium sp. antioxidant compounds*

As part of the continuing exploration for bioactive natural products from an in-house marine macroalgal and cyanobacterial extract library, over 2,800 crude extracts and fractions from samples collected from the Indian, Indo-Pacific, Central and South Pacific, and Western Atlantic (Caribbean) oceans (Luzzatto-Knaan et al., 2017), were evaluated in a 2,2-diphenyl-1-picrylhydrazyl (DPPH) free radical assay. A fraction from the red alga *Ceramium* sp. (Fig. S1), collected in Key West, Florida on May 5, 2001 [fraction 1810E, produced by eluting with 40% hexanes/60% EtOAc from normal phase vacuum liquid chromatography (VLC) of the crude extract] showed potent antioxidant activity, scavenging free radical by 62.0% ± 2.0% at 25 μg/mL. Positive ion LC-ESIMS profile of an active sub-fraction, 1810E-II (27.6 mg), showed a number of

peaks with an isotopic pattern typical for di-brominated and tetra-brominated molecules. GNPS MS2-based molecular networking disclosed the close relationship of these new compounds as well as their novelty within the GNPS libraries (Fig. 2). Further reverse phase VLC and repeated preparative HPLC on C-18 columns, followed by characterization using MS, NMR, and other spectroscopic methods, led to the isolation and characterization of one monomeric (lanosol isopropyl ether, **1**) and seven dimeric bromophenols (bromourceolatols A−G, **2**−**8**).

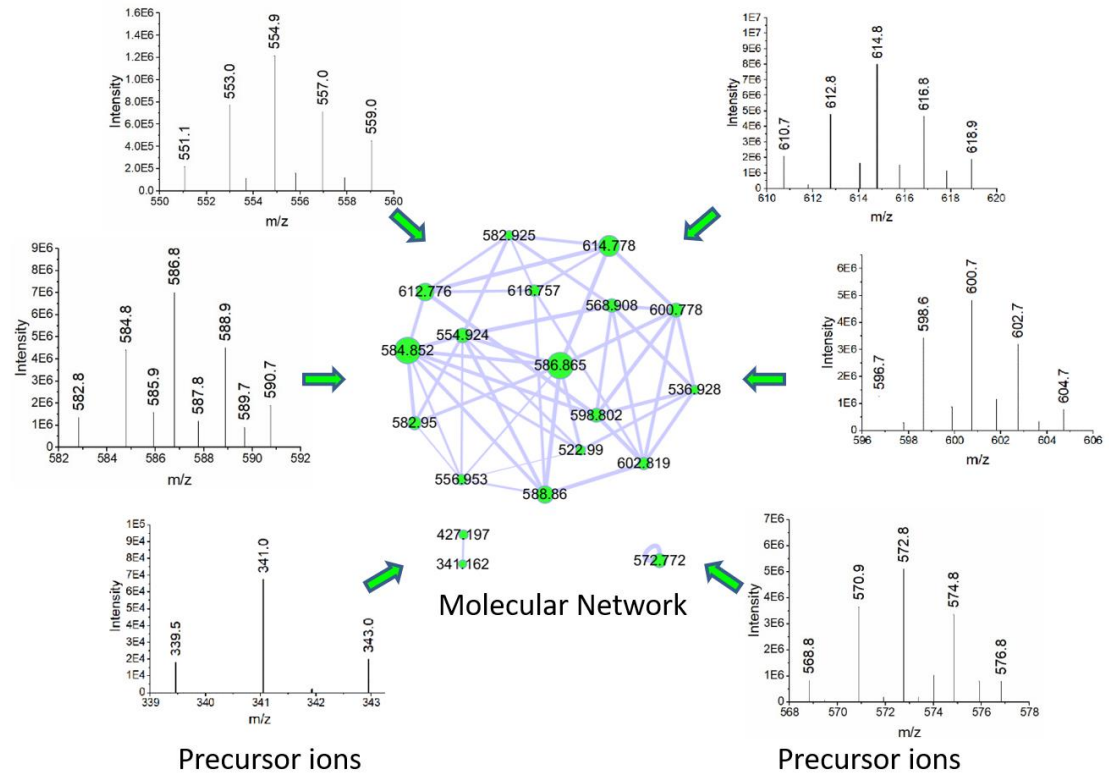


**Fig**. **2**. Positive ion LC-MS$^2$ based molecular network of brominated compounds located within an antioxidant subfraction, 1810E-II of the extract of a *Ceramium* sp.

*2.Structural elucidation of compounds **1**−**8***

Compound **1**, UV$\lambda_{max}$ (MeCN-$H_2O$) 223, 237, and 292 nm, was obtained as a brownish oil and gave a molecular formula of $C_{10}H_{12}Br_2O_3$ by analysis of the

deprotonated molecular ion peak at *m/z* 336.9080 ([M-H]$^-$, $C_{10}H_{11}{}^{79}Br_2O_3^-$, calcd. 336.9080) by HR-ESI$^-$-MS, indicating 4 degrees of unsaturation. Compared with the positive ionization mode, ESI (-)-MS gave a much more intense isotopic cluster for the deprotonated molecular ion for this dibrominated molecule (and for the other compounds reported in this work, see Supplementary Data Fig. S2–Fig. S9). An isopropyl ether was suggested by $^1$H NMR resonances at $\delta_H$ 3.76 (1H, m, H-1') and 1.27 (6H, d, $J$ = 6.1 Hz, $H_3$-2' and $H_3$-3') with attendant $^{13}$C NMR shifts at $\delta_C$ 72.4 (C-1') and 22.2 (C-2' and C-3') (Table S1). A benzyl ether was also in evidence by a deshielded methylene at $\delta_H$ 4.49 (2H, s, H-7) and associated carbon at $\delta_C$ 70.7 (C-7). The only remaining proton signal at $\delta_H$ 7.02 (1H, s, H-6) with an associate carbon at $\delta_C$ 115.7 (C-6), in consideration of the molecular formula, suggested a penta-substituted aromatic ring. Consideration of these structural elements along with the remaining unassigned carbon shifts [$\delta_C$ 143.6 (C-1), 141.3 (C-2), 113.5 (C-3), 114.5 (C-4), 132.1 (C-5)], in relation to the literature for red algal metabolites, suggested that it was closely related to bis(2,3-dibromo-4,5-dihydroxybenzenyl) ether (Kurihara et al., 1999), a dimer of lanosol which is common in red algae (Pedersen et al., 1974). The isopropyl group was connected to C-7 by HMBC correlations from H-7 to C-1' and from $H_2$-1' to C-7 (Fig. 3), thus completing the structure of compound **1** as the previously undescribed isopropyl ether of lanosol, named here as lanosol isopropyl ether.

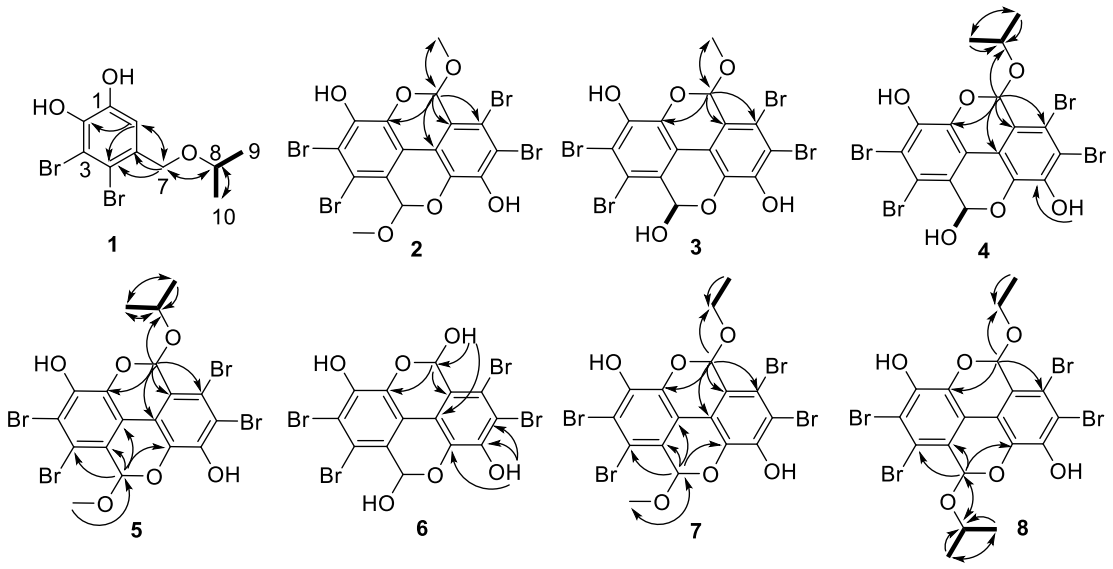

**Fig**. **3**. The key HMBC (arrows) and COSY (bold bonds) correlations of compounds **1**−**8**.

Compound **2**, UV $\lambda_{max}$ (MeCN-$H_2O$) 241, 293, and 330 nm and $[\alpha]_D^{25}$ +1.86 (*c* 0.5, MeOH) and −0.37 (*c* 0.5, acetone), was obtained as a colorless waxy oil and gave a molecular formula of $C_{16}H_{10}Br_4O_6$, as revealed by the deprotonated molecular ion peak at *m/z* 612.7139 ($[M-H]^-$, $C_{16}H_9{}^{79}Br_4O_6^-$ calcd. 612.7138) by HR-ESI-MS, indicating 10 degrees of unsaturation. Intriguingly, the $^1$H NMR spectrum showed only two resonances whereas the $^{13}$C NMR was comprised of eight resonances (Table S1), indicating that it was a symmetric structure. Detailed analysis of the NMR data revealed its similarity to two tetracyclic bromobenzaldehyde dimers 2,7-dibromo-3,8-dihydroxy-5,10-dimethoxyl-5,10-dihydrochromeno[5,4,3-cde]chromenes **2a** (5*S*, 10*S*) and **2b** (5*R*,10*R*) (Liu et al., 2009; Liu et al., 2006), except that two aromatic protons were replaced by two bromine atoms in compound **2**. This deduction was supported by the molecular formula as well as by HMBC correlations from two acetal protons at $\delta_H$ 6.29 (2H, s, H-10 and H-5) to carbons $\delta_C$ 116.9 (C-1 and C-6), 114.9 (C-10a and C-5a), 120.6 (C-10b and C-10c), 136.1 (C-8a and C-3a), and 57.2 (C-1' and C-1")

(Fig. 3). Thus, the planar structure of **2** was determined to be a tetrabrominated analog of **2a** and **2b**, and named bromourceolatol A. The absolute configuration of **2b** (5*R*,10*R*) (62 mg were obtained) was determined by X-ray crystallography, and the specific optical rotation was $[\alpha]_D^{20}$ −2 (*c* 0.367, acetone) (Liu et al., 2006). The absolute configuration of **2a** (5*S*, 10*S*) was deduced by comparison of experimental $^{13}C$ NMR chemical shifts slightly different with the calculated ones by DFT methods using both **2a** and **2b**; however, no optical rotation data had been reported for **2a** (Liu et al., 2009). With the very limited amount of isolated compound **2** (1.2 mg), its weak optical rotation ($[\alpha]_D^{25}$ −0.37 (*c* 0.5, acetone)), CD curve close to zero (see Supplementary), and no known analog with the same planar structure, the absolute configuration of **2** is not easily determined. However, the 5*S*,10*R*- and 5*R*,10*S*-possibilities can be ruled out because an asymmetric structure would be expected to have 16 distinct carbon resonance signals (Liu et al., 2009).

Compound **6**, showing UV $\lambda_{max}$ (MeCN-$H_2O$) 241, 293, and 331 nm and $[\alpha]_D^{25}$ −1.81 (*c* 0.5, MeOH) and −0.45 (*c* 0.5, acetone), was obtained as a light yellow waxy oil. A molecular formula of $C_{14}H_6Br_4O_6$ was deduced by analysis of the deprotonated HR-ESI-MS molecular ion peak at *m/z* 588.6776 ($[M-H]^-$, $C_{14}H_5{}^{79}Br_2{}^{81}Br_2O_6^-$ calcd. 588.6785), indicating 10 degrees of unsaturation. The NMR data for compound **6** (Table S1) indicated a symmetrical structures with only 7 carbon resonances, similar to compound **2** except for the absence of the two methoxy resonances and the presence of an additional 2H hydroxy signal at $\delta_H$ 7.93 (d, *J* = 6.0 Hz, 10-OH and 5-OH). These data suggested that **6** was the demethylated analog of **2**, and was given the name

bromourceolatol E. The structure of **6** was further supported by HMBC correlations from 10-OH (5-OH) to C-10 (C-5) and C-10b (C-10c), and from the phenol hydroxyl protons 3-OH (8-OH) to C-2 (C-7), C-3 (C-8), and C-3a (C-8a) (Fig.3). Considering its high structural similarity and co-occurrence with compound **2**, the configuration of **6** is likely also 5*R*,10*R* or 5*S*,10*S*.

Compound **3**, named bromourceolatol B, UV $\lambda_{max}$ (MeCN-$H_2O$) 239, 293, and 331 nm and $[\alpha]_D^{25}$ −0.13 (*c* 0.5, MeOH) and −1.23 (*c* 0.5, acetone), was obtained as a colorless waxy oil and gave a molecular formula of $C_{15}H_8Br_4O_6$, as revealed by the deprotonated molecular ion peak at *m/z* 598.6975 ($[M-H]^-$, $C_{15}H_7{}^{79}Br_4O_6^-$ calcd. 598.6982; 10 degrees of unsaturation). The NMR data of **3** (Table S2) showed that it was an asymmetric molecule and possessed a single methoxy group ($\delta_H$ 3.64 ($H_3$-1'), $\delta_C$ 56.0 (C-1')) compared with compound **2**. This was also confirmed by HMBC correlations from $H_3$-1' to C-10, C-10a, C-1, and C-8a (Fig. 3). The presence of a hydroxy group at C-5 was supported by a COSY correlation between the OH proton ($\delta_H$ 6.94, $J$ = 5.8 Hz) and H-5 ($\delta_H$ 6.68, $J$ = 5.8 Hz). This formed a hemiacetal carbon as revealed by the distinctive $^{13}C$ NMR shift of C-5 at $\delta_C$ 93.9.

Compound **4**, given the name bromourceolatol C, with UV $\lambda_{max}$ (MeCN-$H_2O$) 237, 294, and 331 nm and $[\alpha]_D^{25}$ +0.90 (*c* 0.5, MeOH) and +1.91 (*c* 0.5, acetone), was obtained as a light yellow waxy oil. By HRMS, it gave a molecular formula of $C_{17}H_{12}Br_4O_6$, with a deprotonated molecular ion peak at *m/z* 626.7287 ($[M-H]^-$, $C_{17}H_{11}{}^{79}Br_4O_6^-$ calcd. 626.7295; 10 degrees of unsaturation). Compared with compound **3**, its NMR spectrum was different only in that the methyl group in **3** was replaced by

an isopropyl group in **4** (Table S2). This was suggested by a series of isopropyl resonances [$\delta_H$ 4.34 (H-1', m), 1.34 ($H_3$-2', d, $J$ = 6.2 Hz), 1.21 ($H_3$-3', d, $J$ = 6.2 Hz); $\delta_C$ 73.0 (C-1'), 22.1 (C-2'), 23.8 (C-3')] that were connected by numerous COSY and HMBC correlations (Fig. 3). A broadened hydroxy proton (5-OH, $\delta_H$ 3.66) showed a COSY correlation with a hemiacetal proton H-5 ($\delta_H$ 6.75, d, $J$ = 4.6 Hz); again, the distinctive $^{13}$C NMR shift of C-5 ($\delta_C$ 93.2) confirmed the nature of this functional group, and completed the structural characterization of compound **4**.

Compound **5**, UV $\lambda_{max}$ (MeCN-$H_2O$) 241, 293, and 330 nm and $[\alpha]_D^{25}$ −1.85 ($c$ 0.5, MeOH) and +0.33 ($c$ 0.5, acetone), was obtained as a colorless waxy oil. In HR-ESI-MS it showed a deprotonated molecular ion peak at *m/z* 644.7407 ([M-H]$^-$, $C_{18}H_{13}{}^{79}Br_2{}^{81}Br_2O_6^-$ calcd. 644.7412) for a molecular formula of $C_{18}H_{14}Br_4O_6$, indicating 10 degrees of unsaturation. In addition to the isopropoxy resonances seen in compound **4**, the NMR spectra of **5** showed an additional methoxyl group (Table S2) with signals at $\delta_H$ 3.64 (H-1", s) and $\delta_C$ 56.8 (C-1"). The structure of **5** was supported by the HMBC correlations from H-1" to C-5 ($\delta_C$ 99.9), and from H-5 ($\delta_H$ 6.29, s) to C-6, C-5a, C-10c, and C-3a, and from H-10 ($\delta_H$ 6.46, s) to C-1', C-1, C-10a, C-10b, and C-8a (Fig. 3). The structure of compound **5** was thus completed and given the trivial name of bromourceolatol D.

Compound **7**, UV $\lambda_{max}$ (MeCN-$H_2O$) 241, 293, and 330 nm and $[\alpha]_D^{25}$ +1.47 ($c$ 0.5, MeOH) and +0.33 ($c$ 0.5, acetone), was also obtained as a colorless waxy oil and gave a molecular formula of $C_{17}H_{12}Br_4O_6$, as revealed by deprotonated-molecular ion peak at *m/z* 626.7291 ([M-H]$^-$, $C_{17}H_{11}{}^{79}Br_4O_6^-$ calcd. 626.7295) by HR-ESI-MS. This

again indicated 10 degrees of unsaturation. Compared with compound 5, compound 7 was very similar and also possessed a methoxy group. However, the resonances for the isopropyl group in compound **5** were replaced by those of an ethoxy moiety in **7**. This was reflected by two sets of signals for the ethoxy group at ($\delta_H$ 3.91 and 4.05 ($H_2$-1', m), 1.18 ($H_3$-2', t, $J$ = 7.1 Hz); $\delta_C$ 64.9 (C-1'), 14.7 (C-2')) (Table S2). The structure of **7**, given the trivial name of bromourceolatol F, was supported by the HMBC correlations from H-2' to C-1', from H-10 ($\delta_H$ 6.40, s) to C-1', C-1, C-10a, C-10b, and C-8a, and from H-5 ($\delta_H$ 6.29, s) to C-1", C-6, C-5a, C-10c, and C-3a (Fig. 3).

Compound **8**, UV $\lambda_{max}$ (MeCN-$H_2O$) 239, 293, and 330 nm and $[\alpha]_D^{25}$ +1.31 (*c* 0.5, MeOH) and -2.71 (*c* 0.5, acetone), was obtained as a light yellow waxy oil and gave by HR-ESI-MS a molecular formula of $C_{19}H_{16}Br_4O_6$. This was revealed by a deprotonated molecular ion peak at *m/z* 658.7569 ($[M-H]^-$, $C_{19}H_{15}{}^{79}Br_2{}^{81}Br_2O_6^-$ calcd. 658.7568), and again indicated,10 degrees of unsaturation. Compared with compound **7**, the methoxy was replaced by an isopropoxy in **8**, as reflected by three sets of signals ($\delta_H$ 4.35 (H-1", m), 1.25 ($H_3$-2", t, $J$ = 6.2 Hz), 1.05 ($H_3$-3", t, $J$ = 6.2 Hz); $\delta_C$ 70.6 (C-1"), 21.0 (C-2"), 22.9 (C-3")) (Table S2). The structure of **8** with its ethoxy and isopropoxy groups was supported by HMBC correlations from H-5 ($\delta_H$ 6.34, s) to C-1", C-6, C-5a, and C-3a, from H-2' to C-1', and from H-10 ($\delta_H$ 6.27, s) to C-1', C-1, and C-8a (Fig. 3). Compound **8** was given the trivial name bromourceolatol G.

Compounds **2**−**8** were present in quite small amounts and had weak optical rotations and CD curves; therefore, their absolute configurations could not be deduced, but perhaps may be resolved in the future by new and innovative approaches such as

MicroED (Jones et al., 2018).

We suggest that the tetracyclic skeleton of compounds **2−7** are produced via a similar biosynthetic pathway to that of compound **2b** (Liu et al., 2006). The potential precursor to these polycyclic compounds is predicted to be 2,3-dibromo-4,5-dihyroxybenzaldehyde, a metabolite that is broadly present in red alga (Li et al., 2011; Olsen et al., 2013; Pedersen et al., 1974; Wang et al., 2013). This was found to be present in small quantity in this *Ceramium* sp. extract as revealed by a dibrominated [M-H]- isotopic cluster (m/z 293.05/295.05/296.90) in the LC-MS profile of sub-fraction 1810E-II (Supplementary Information, Fig. S48). This precursor is hypothesized to dimerize between the α-C atoms via the well-known radical coupling reaction for phenols (Jian-Zhong Wu et al., 2007; Liu et al., 2006). Subsequently, condensation between each OH group and each CHO group of the opposite monomer yields the two pyrone rings, such as seen for compound **6** (Fig. 4). Because brominated compounds with a similar teracyclic system were previously reported from red alga in the order Ceramiales (Li et al., 2008; Liu et al., 2009; Liu et al., 2006), we propose compound **6** to be a true natural product. The other compounds (**2**−**5** and **7**−**8**) may be formed via alkylation by alcohols or biogenetic alkyl donors like S-adenosylmethionine (SAM); this will require further investigation.

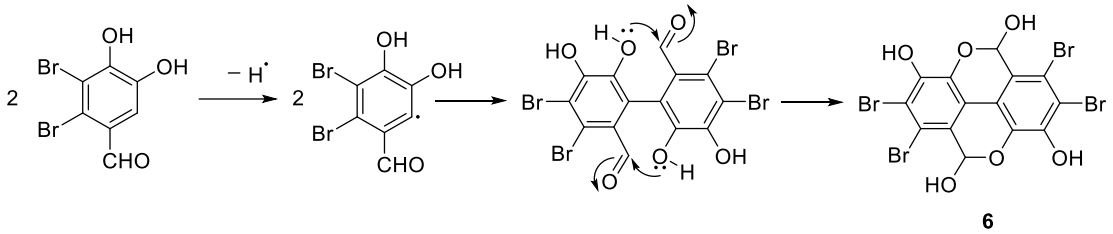


**Fig**. **4**. The hypothetic biogenetic pathway of compound **6**.

*2.3. Bioactivity study*

The DPPH assay revealed that all of the isolated *Ceramium* sp. compounds possessed antioxidant activity. Among them, compounds **1** and **3** displayed similar activity with scavenging $EC_{50}$ to DPPH free radical of 44.4±0.3 μM and 47.0±6.0 μM, respectively, close to the positive control of vitamin C ($EC_{50}$: 36.2±1.3 μM) and a little weaker thn trolox ($EC_{50}$: 15.9±1.5 μM). Since the rest of the compounds did not reach the full scavenging effect at the screened doses, their curves are not S-shaped and we were not able to assess their exact EC50 values, just to establish their approximate values: ~ 64 μM for compounds **2** and **4**, ~96 μM for compounds **5** and **8**; ~128 μM for compounds **6** and **7**. (Fig. 5).

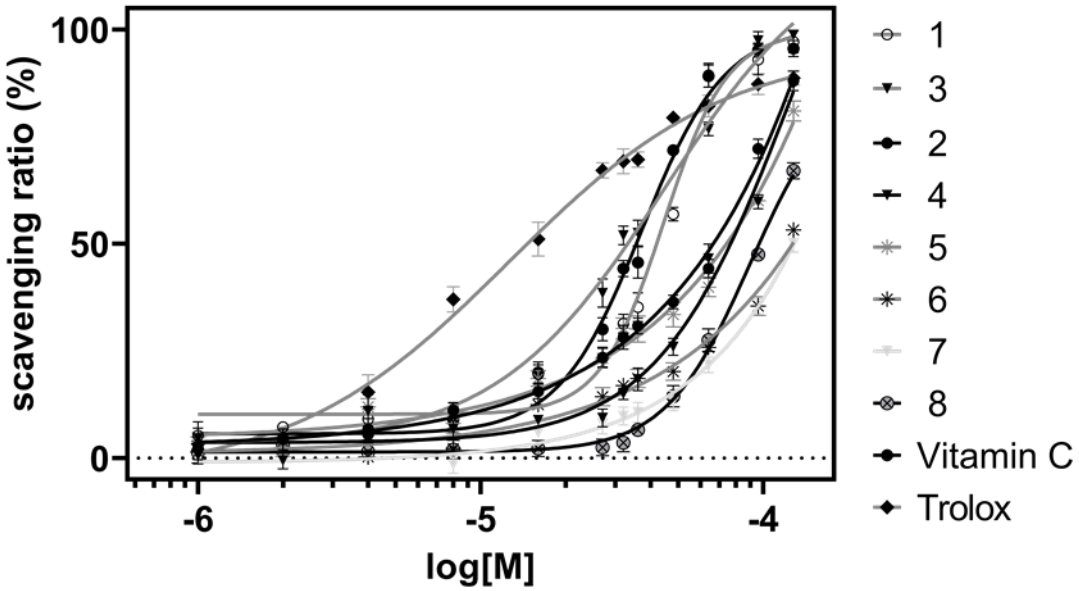


**Fig**. **5**. The DPPH free radical scavenging activity of compounds compound **1−8**. $EC_{50}$ values were calculated using Prism Graphpad software (n = 3) with variable slopes.

Furthermore, the new *Ceramium* sp. compounds were also tested for anti-inflammatory activity using the LPS-induced RAW 264.7 macrophage cell system and two concentrations of potential inhibitor (16 and 32 μM). Only at the higher doze,

compounds **2**, **3**, and **7** exhibited significant inhibition of LPS-induced NO production (inhibition by 97%, 47%, and 73%, respectively, Fig. 6). At these concentrations, these compounds were not overtly cytotoxic to these cells, although compound **2** also showed some cytotoxicity; nevertheless, its anti-inflammatory effect was much stronger than its cytotoxicity.

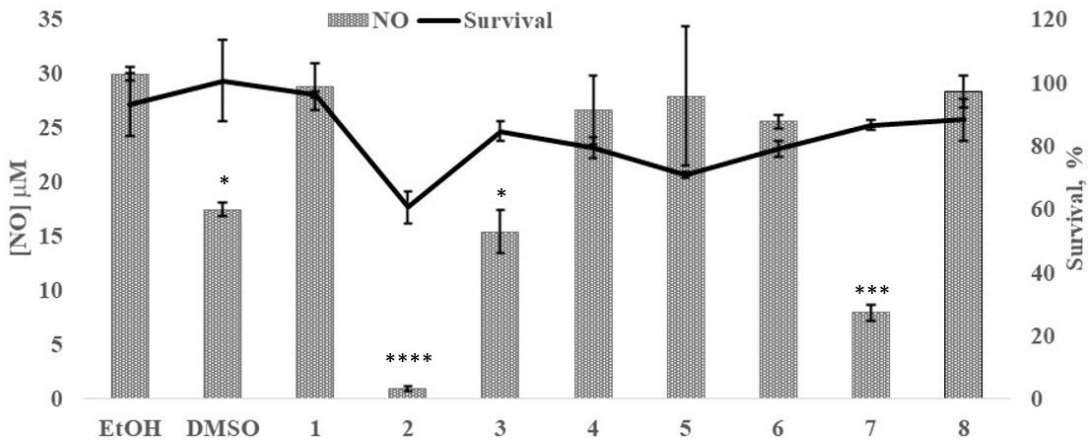


**Fig. 6**. Evaluation of cytotoxicity (line) and inhibition of LPS-induced NO production (bars) by compound **1−8** at 32 µM (no activity was observed at 16 µM). Ethanol (1%) alone served as the negative control, and DMSO (0.75%) was used as the positive control. (n = 3; ****, *** and * represent adjusted P values of <0.0001, 0.0005, and 0.05, respectively). One-way ANOVA followed by Tukey's multiple comparisons test was performed using GraphPad Prism version 8.0.0 for Windows. Amount of NO production calculated from a standard curve (see Supporting Information).

Considering the activity of compounds **2**, **3**, and **7** in both the antioxidant and anti-inflammatory assay, we propose that their anti-inflammatory activity may involve an antioxidant mechanism; however, more than one mechanism seems likely as their rank order of potency differed in the two assays. Additionally, due to the very small amounts of isolated natural products in this study (0.5 to 1.5 mg), there remains the possibility of weigh errors such that consideration of structure-activity relationships would constitute an overreach of the data and its quality.

However, the available literature for bromophenol natural products, including

compounds structurally similar to molecules **1**−**8**, indicate that they have a diversity of biological activities. For example, lanosol and several of its analogs, similar to compound **1**, displayed antifeedant activity, inhibition to a rice fungal pathogen, allelopathic effects to algae, inhibition to α-glucosidase, sucrase and maltase, and antitumor properties (Jesus et al., 2019; Wang et al., 2013). Additionally, tetracyclic bromophenols structurally related to compounds **2**−**8**, also isolated from red alga, were found to possess antibacterial, anti-scuticociliate (a marine ciliate in the class Oligohymenophorea), and antitumor activities; the latter targeting protein tyrosine kinase and the C-kit receptor (Kang et al., 2014; Shi et al., 2009). Thus, the biological potential of the compounds isolated in present study deserve further examination, but will likely require chemical synthesis in order to provide the needed compound supply.

## 3. Conclusion

An antioxidant bioassay and LC-$MS^2$-based GNPS analysis guided the isolation and structure elucidation of one new brominated phenol monomer (**1**) and seven new tetracyclic dimers (**2**−**8**), all of which displayed antioxidant and anti-inflammatory activities. This report significantly expands on previous reports of bromophenols isolated from the genus *Ceramium* which previously was only known to contain lanosol (Phillips et al, 1981) and several less well characterized polybrominated diphenyl ethers (PBDEs) (Dalgren et al., 2015). Continued investigation of the absolute configurations and other biological activities of the newly isolated compounds is ongoing.

## 4. Experimental

### *4.1 General Experimental Procedures*

1D and 2D NMR spectra were recorded on a JEOLECZ-500R NMR spectrometer (Tokyo, Japan) or on a Bruker Advance 600 MHz NMR spectrometer (Billerica, MA, USA) using tetramethylsilane as an internal standard. For all the compounds, regular 8 Hz optimized HMBC were used although some were also measured using a 2 Hz optimized HMBC. HR-ESI-MS spectra were obtained using an Agilent 6230 Accurate-Mass TOFMS mass spectrometer (Santa Clara, USA) under negative ion mode. The optical rotation was measured on a JASCO P-2000 polarimeter (Easton, MD, USA). The circular dichroism (CD) experiment was performed on an Aviv Model 215 circular dichroism spectrometer (Lakewood, USA). An INTEGRA VIAFLO 96 system (Hudson, USA) was used to run semi-automatic pipetting manipulation during the high throughput antioxidant bioassay. A Molecular Device Spectromax M2 microplate reader (Winooski, VT, USA) was used for all colorimetric measurements. A Büchi R-114 Rotavapor (Flawil, Switzerland) was used for sample preparation. All nominal mass resolution LC-MS analyses were run on a Phenomenex Kinetex C18 100A reverse phase column (100 × 4.60 mm, 5 μm) using a Thermo Finnigan Surveyor Autosampler-Plus/LC-Pump-Plus/PDA-Plus system and a Thermo Finnigan LCQ Advantage Plus mass spectrometer. Preparative HPLC were run on a Kinetex C18 semi-preparative column (150 × 10.0 mm, 5 μm, Phenomenex) or a YMC C18 column (YMC-Pack Pro C18 RS, 5 μm) using an Thermo Fisher Scientific Ultimate 3000 UHPLC system (Waltham, USA) with a diode array detector. Vacuum liquid chromatography were

performed using silica gel (type H, 10−40 μm, Sigma-Aldrich) and C18 SPE (5000 mg/20 mL, SEClute). All solvents were HPLC grade products from Thermo Fisher Scientific.

*4.2 Library samples and the macroalga Ceramium sp.*

The marine samples used for the antioxidant assay were derived from cyanobacteria and macro-algae which were collected from locations in the Indian, Indo-Pacific, Central and South Pacific, and Western Atlantic (Caribbean) oceans. Following a standard protocol, all samples were repeatedly extracted with $CH_2Cl_2$/MeOH (2:1) and fractionated into nine fractions (A−I) by silica gel vacuum liquid chromatography using a stepwise gradient of hexanes/EtOAc and EcOAc/MeOH. All crude extracts and fractions were dissolved in DMSO and stored in 96-well plates as a sample library at -20$^{o}$ C until use (Luzzatto-Knaan et al., 2017).

The species used in the present chemical study was collected at the intertidal zone of Key West, Florida, USA (N 24°33'04.0", W 81°46'38.0"; depth) in 2001. The biomass and specimen voucher were preserved in 1:1 seawater/2-propanol solution at -20$^{o}$ C until use. The species was identified by light microscopy using the unique branched morphology (insert reference above) of the well-preserved filaments (see Fig. S1 in Supplementary data) as a filamentous macroalgae of the genus *Ceramium* (Rhodophyta, Ceramiales) (Meneses, 1995). The light microscope employed was an Evos XL Core Imaging System.

*4.3 The DPPH antioxidant assay*

The antioxidant assay used 2,2-diphenyl-1-picrylhydrazyl (DPPH)(Fisher Scientific)

and was performed using a previously described 96-well microplate colormetric method (Yang et al., 2018). Samples were diluted with MeOH and the final concentration in the reaction system was 25 μg/ml. Each sample was tested in three replicates and the values were averaged to obtain calculated scavenging ratios to DPPH. For the assessment of activity of the pure compounds, a series of concentrations from 0.125 to 128 μM were evaluated. Trolox and vitamin C were used as positive controls. Dose curves were plotted and semi-scavenging concentrations ($EC_{50}$) were calculated by GraphPad Prism version 8.0.0 for Windows, GraphPad Software, San Diego, California USA, www.graphpad.com with variable slopes.

*4.4 Extraction, Molecular Networking, and Compound Isolation*

The frozen biomass was warmed to room temperature, and then following the protocol described in part 4.2, the biomass was extracted to give a crude extract (Serial number 1810, 3.13 g) that was further fractionated by silica gel VLC to afford fractions 1810A−1810I. These were used for populating the above described library and also for samples for chemical investigation. Fraction 1810E (40% hexanes/60% EtOAc eluent, 148 mg) showed DPPH scavenging ratio of 62.02%±2.03% at 25 μg/ml, and was thus subject to further fractionation using a SPE C18 column and a stepwise gradient elution of MeOH/$H_2O$ (40:60 to 100:0), MeOH/acetone (50:50), acetone, and finally $CH_2Cl_2$ to yield four sub-fractions 1810E-I to 1810E-IV. Antioxidant activity of these fractions revealed an active sub-fraction 1810E-II (60:40-70:30 MeOH/$H_2O$ eluent, 27.6 mg). LC-$MS^2$ of this fraction showed the presence of unique brominated compounds.

The LC-$MS^2$ analysis was run on the LC-PDA-$MS^2$ system described above by monitoring UV 190−600 nm and *m/z* 100−2000 in positive ion mode (the unified mode for GNPS molecular networking). The detailed MS detector setting include: default charge state = 1, default isolation width = 2, normalized collision energe = 35 eV, minimal signal required = 100,000, ion source voltage = 4 kV, capillary temperature = 325 °C, capillary voltage = 10 V. The concentration of the fraction was adjusted to 0.15 mg/ml in MeOH and the injection volume was 25 μL. The flow rate was set to 0.6 mL/min and a gradient program of $CH_3CN/H_2O$ containing 0.1% formic acid was used for elution: 0−2 min for 40% $CH_3CN$, 2−22 min for 40% to 99% $CH_3CN$, 22−26 min for 99% $CH_3CN$, 26−26.5 min for 99% to 40% $CH_3CN$, 26.5−30 min for 40% $CH_3CN$. The MS/MS spectra from this sample were used to generate a molecular network using the GNPS Web site and visualized using Cytoscape 3.7 software for the purpose of dereplication and molecular targeting. The raw data have been uploaded to the MassIVE Database at the GNPS Web site (https://gnps.ucsd.edu/ProteoSAFe/static/gnps-splash.jsp) (Wang et al, 2016) and is publicly available through access number MSV000084691. The link for this molecular networking job is https://gnps-cytoscape.ucsd.edu/process?task=4c5fde81f1ac4381a89e13a00f592cde.

The subfraction 1810E-II was further separated by preparative HPLC (pHPLC) on a Kinetex C18 semi-preparative column eluted with $CH_3CN/H_2O$ (0−22.0 min, 55% $CH_3CN$; 22.0−22.5 min, 55%−99% $CH_3CN$; 22.5−26.5 min, 99% $CH_3CN$; 26.5−27.0 min, 99% −55% $CH_3CN$; 27.0−30.0 min, 55% $CH_3CN$; flow rate = 2 mL/min) to afford

fractions 1810E-II-1 (7.5−10.3 min, 17.2 mg), -2 (10.6−12.5 min, 4.9 mg), -3 (12.6−17.3 min, 5.0 mg), -4 (17.3−20.7 min, 2.3 mg), -5 (20.7−23.5 min, 2.8 mg) and -6 (25.2−27.5 min, 3.3 mg).

Fraction 1810E-II-1 was sequentially separated by pHPLC on the same column eluted with $CH_3CN/H_2O$ (0−25.0 min, 42% $CH_3CN$; 25.0−27.0 min, 42%−99% $CH_3CN$; 27.0−35.0 min, 99% $CH_3CN$; 35.0−35.5 min, 99%−42% $CH_3CN$; 35.5−40.0 min, 42% $CH_3CN$; flow rate = 2 mL/min) to give compound **1** (16.2−19.3 min, 9.0 mg), compound **2** (30.0−30.7 min, 1.2 mg), fraction 1810E-II-1-4 (21.1−24.4 min, 2.4 mg), and other minor fractions. From 1810E-II-1-4, by successive pHPLC purification first on the same column eluted with 42% $CH_3CN$ and secondly on the YMC C18 column eluted with 60% $CH_3CN$, compound **3** (1.7 mg) was obtained. Fraction 1810E-II-2 was separated by pHPLC on the Kinetex C18 column eluted with $CH_3CN/H_2O$ (0−38.0 min, 42% $CH_3CN$; 38.0−40.0 min, 42%−99% $CH_3CN$; 40.0−45.0 min, 99% $CH_3CN$; 45.0−45.5 min, 99%−42% $CH_3CN$; 45.5−50.0 min, 42% $CH_3CN$; flow rate = 2.5 mL/min) to provide a minor fraction 1810E-II-2-1 and a main one 1810E-II-2-2 (30.0−37.4 min, 4.0 mg). From 1810E-II-2-2, compounds **4** (16.9−19.2 min, 1.1 mg) and **5** (26.6−27.9 min, 0.3 mg) were obtained by pHPLC on the YMC C-18 column eluted with $CH_3CN/H_2O$ (0−20.0 min, 67% $CH_3CN$; 20.0−21.0 min, 67%−99% $CH_3CN$; 21.0−30.0 min, 99% $CH_3CN$; 30.0−31.0 min, 99%−67% $CH_3CN$; 31.0−37.0 min, 67% $CH_3CN$; flow rate = 2.0 mL/min). 1810E-II-3 was separated by alternating pHPLC purification first on the YMC C-18 column eluted with 63% $CH_3CN$ (2.5 mL/min), then on the Kinetex C18 column (45% $CH_3CN$, 2.0 mL/min), and finally on the YMC C18 column

(65% $CH_3CN$, 2.0 mL/min) to yield compound **6** (1.5 mg). Fraction 1810E-II-4 was separated on the YMC C18 column eluted with $CH_3CN/H_2O$ (0−18.0 min, 75% $CH_3CN$; 18.0−19.0 min, 75%−99% $CH_3CN$; 19.0−24.0 min, 99% $CH_3CN$; 24.0−24.5 min, 99%−75% $CH_3CN$; 24.5−30.0 min, 75% $CH_3CN$; flow rate = 2.0 mL/min) to provide compound **7** (16.7−18.7 min, 1.5 mg). Fraction 1810E-II-6 was separated on the Kinetex C18 column eluted with $CH_3CN/H_2O$ (0−22.0 min, 60% $CH_3CN$; 22.0−23.0 min, 60%−99% $CH_3CN$; 23.0−29.5 min, 99% $CH_3CN$; 29.5−30.5 min, 99%−60% $CH_3CN$; 30.5−35.0 min, 60% $CH_3CN$; flow rate = 2.0 mL/min) to provide compound **8** (16.3−18.1 min, 1.0 mg).

Lanosol isopropyl ether (**1**): Brownish oil. UV $\lambda_{max}$ (MeCN-$H_2O$) 223, 237, and 292 nm. $^1H$ and $^{13}C$ NMR data: see Table S1. HR-ESI$^-$-MS: *m/z* 336.9080 $[M-H]^-$ ($C_{10}H_{11}{}^{79}Br_2O_3^-$ calcd. 336.9080), 338.9058 $[M+2-H]^-$, 340.9042 $[M+4-H]^-$ (with abundance ratio of 1:2:1). LR-ESI$^-$-MS: see details for $[M-H]^-$ isotopic patterns in Fig. S2.

Bromourceolatol A (**2**)**:** Colorless waxy oil. UV $\lambda_{max}$ (MeCN-$H_2O$) 241, 293, and 330 nm. $[\alpha]_D^{25}$ +1.86 (*c* 0.5, MeOH) and −0.37 (*c* 0.5, acetone). CD: see Fig. S47. $^1H$ and $^{13}C$ NMR data: see Table S1. HR-ESI$^-$-MS: *m/z* 612.7139 $[M-H]^-$ ($C_{16}H_9{}^{79}Br_4O_6^-$ calcd. 612.7138), 614.7118 $[M+2-H]^-$, 616.7097 $[M+4-H]^-$, 618.7081 $[M+6-H]^-$, 620.7063 $[M+8-H]^-$ (with abundance ratio of 1:4:6:4:1). LR-ESI$^-$-MS: see details for $[M-H]^-$ and $[M-H-CH_3OH]^-$ isotopic patterns in Fig. S3; *m/z* 584.80 $[M-H-CH_3OH]^-$ in $MS^2$ of base peak ion. LR-ESI$^+$-MS: see details for $[M+H-CH_3OH]^+$ and [M+H−

$2CH_3OH]^+$ isotopic patterns in Fig. S3; *m/z* 554.86 $[M+H-2CH_3OH]^+$ in $MS^2$ of base peak ion.

Bromourceolatol B (**3**)**:** Colorless waxy oil. UV $\lambda_{max}$ (MeCN-$H_2O$) 239, 293, and 331 nm. $[\alpha]_D^{25}$ −0.13 (*c* 0.5, MeOH) and −1.23 (*c* 0.5, acetone). CD: see Fig. S47. $^1H$ and $^{13}C$ NMR data: see Table S2. HR-ESI$^-$-MS: *m/z* 598.6975 $[M-H]^-$ ($C_{15}H_7{}^{79}Br_4O_6^-$ calcd. 598.6982) , 600.6951 $[M+2-H]^-$, 602.6930 $[M+4-H]^-$, 604.6931 $[M+6-H]^-$, 606.6903 $[M+8-H]^-$ (with abundance ratio of 1:4:6:4:1). LR-ESI$^-$-MS: see details for $[M-H]^-$ and $[M-H-CO]^-$ isotopic patterns in Fig. S4; m/z 574.88 $[M-H-CO]^-$ in $MS^2$ of base peak ion. LR-ESI$^+$-MS: see details for $[M+H-H_2O]^+$, $[M+H-H_2O-CO]^+$, and $[M+H-H_2O-CH_3OH]^+$ isotopic patterns in Fig. S4; m/z 554.89 $[M+H-H_2O-CH_3OH]^+$ in $MS^2$ of base peak ion.

Bromourceolatol C (**4**)**:** light yellow waxy oil. UV $\lambda_{max}$ (MeCN-$H_2O$) 237, 294, and 331 nm. $[\alpha]_D^{25}$ +0.90 (*c* 0.5, MeOH) and +1.91 (*c* 0.5, acetone). CD: see Fig. S47. $^1H$ and $^{13}C$ NMR data: see Table S2. HR-ESI$^-$-MS: *m/z* 626.7287 $[M-H]^-$ ($C_{17}H_{11}{}^{79}Br_4O_6^-$ calcd. 626.7295), 628.7267 $[M+2-H]^-$, 630.7249 $[M+4-H]^-$, 632.7232 $[M+6-H]^-$, 634.7221 $[M+8-H]^-$ (with abundance ratio of 1:4:6:4:1). LR-ESI$^-$-MS: see details for $[M-H]^-$ and $[M-H-CO]^-$ isotopic patterns in Fig. S5; *m/z* 602.77 $[M-H-CO]^-$ in $MS^2$ of base peak ion. LR-ESI$^+$-MS: see details for $[M+H-H_2O]^+$ and $[M+H-H_2O-C_3H_6]^+$ isotopic patterns in Fig. S5; m/z 554.93 $[M+H-H_2O-C_3H_6-CO]^+$ in $MS^2$ of base peak ion.

Bromourceolatol D (**5**)**:** Colorless waxy oil. UV $\lambda_{max}$ (MeCN-$H_2O$) 241, 293, and 330 nm. $[\alpha]_D^{25}$ −1.85 (*c* 0.5, MeOH) and +0.33 (*c* 0.5, acetone). CD: see Fig. S47. $^1H$

and $^{13}C$ NMR data: see Table S2. HR-ESI$^-$-MS: *m/z* 640.7548 [M−4−H]$^-$, 642.7427 [M−2−H]$^-$, 644.7407 [M−H]$^-$ ($C_{18}H_{13}{}^{79}Br_2{}^{81}Br_2O_6^-$ calcd. 644.7412), 646.7383 [M+2−H]$^-$, 648.7350 [M+4−H]$^-$ (with abundance ratio of 1:4:6:4:1). LR-ESI$^-$-MS: see details for [M−H]$^-$, [M−H−$CH_3OH$]$^-$ and [M−H−$CH_3OH$−CO]$^-$ isotopic patterns in Fig. S6; *m/z* 612.77 [M−H−$CH_3OH$]$^-$ and 584.70 [M−H−$CH_3OH$−CO]$^-$ in MS$^2$ of base peak ion. LR-ESI$^+$-MS: see details for [M+H−$CH_3OH$]$^+$, [M+H−$CH_3OH$−CO]$^+$, and [M+H−2$CH_3OH$−CO]$^+$ isotopic patterns in Fig. S6; m/z 554.90 and 554.89 [M+H−2$CH_3OH$−CO]$^+$ in MS$^2$ of base peak ions.

Bromourceolatol E (**6):** light yellow waxy oil. UV $\lambda_{max}$ (MeCN-$H_2O$) 241, 293, and 331 nm. $[\alpha]_D^{25}$ −1.81 (*c* 0.5, MeOH) and −0.45 (*c* 0.5, acetone). CD: see Fig. S47. $^1H$ and $^{13}C$ NMR data: see Table S1. HR-ESI$^-$-MS: *m/z* 584.6816 [M−4−H]$^-$, 586.6791 [M−2−H]$^-$, 588.6776 ([M−H]$^-$, $C_{14}H_5{}^{79}Br_2{}^{81}Br_2O_6^-$ calcd. 588.6785), 590.6757 [M+2−H]$^-$, 592.6741 [M+4−H]$^-$ (with abundance ratio of 1:4:6:4:1). LR-ESI$^-$-MS: see details for [M−H]$^-$ and [M−H−2CO]$^-$ isotopic patterns in Fig. S7; *m/z* 560.73 [M−H−CO]$^-$ and 532.86 [M−H−2CO]$^-$ in MS$^2$ of base peak ion. LR-ESI$^+$-MS: see details for [M+H−$H_2O$]$^+$ isotopic patterns in Fig. S7; m/z 554.99 [M+H−$H_2O$ −CO]$^+$ in MS$^2$ of base peak ions.

Bromourceolatol F (**7):** Colorless waxy oil. UV $\lambda_{max}$ (MeCN-$H_2O$) 241, 293, and 330 nm. $[\alpha]_D^{25}$ +1.47 (*c* 0.5, MeOH) and +0.33 (*c* 0.5, acetone). CD: see Fig. S47. $^1H$ and $^{13}C$ NMR data: see Table S2. HR-ESI$^-$-MS: *m/z* 626.7291 ([M−H]$^-$, $C_{17}H_{11}{}^{79}Br_4O_6^-$ calcd. 626.7295), 628.7272 [M+2−H]$^-$, 630.7253 [M+4−H]$^-$, 632.7233 [M+6−H]$^-$, 634.7222 [M+8−H]$^-$ (with abundance ratio of 1:4:6:4:1). LR-ESI$^-$-MS: see details for

$[M-H]^-$ and $[M-H-CH_3OH]^-$ isotopic patterns in Fig. S8; *m/z* 598.75 $[M-H-CH_3OH]^-$ and 584.82 $[M-H-C_2H_5OH]^-$ in $MS^2$ of base peak ion. LR-$ESI^+$-MS: see details for $[M+H-CH_3OH]^+$, $[M+H-C_2H_5OH]^+$, and $[M+H-CH_3OH-C_2H_5OH]^+$ isotopic patterns in Fig. S8; m/z 554.90 $[M+H-CH_3OH-C_2H_5OH]^+$ in $MS^2$ of base peak ion.

Bromourceolatol G (**8):** light yellow waxy oil. UV $\lambda_{max}$ (MeCN-$H_2O$) 239, 293, and 330 nm. $[\alpha]_D^{25}$ +1.31 (*c* 0.5, MeOH) and −2.71 (*c* 0.5, acetone). CD: see Fig. S47. $^1H$ and $^{13}C$ NMR data: see Table S2. HR-$ESI^-$-MS: *m/z* 654.7600 $[M-4-H]^-$, 656.7589 $[M-2-H]^-$, 658.7569 $[M-H]^-$ ($C_{19}H_{15}{}^{79}Br_2{}^{81}Br_2O_6^-$ calcd. 658.7568), 660.7553 $[M+2-H]^-$, 662.7537 $[M+4-H]^-$ (with abundance ratio of 1:4:6:4:1). LR-$ESI^-$-MS: see details for $[M-H]^-$, $[M-H-C_2H_5OH]^-$, and $[M-H-C_3H_7OH]^-$ isotopic patterns in Fig. S9; *m/z* 612.79 $[M-H-C_2H_5OH]^-$ and 598.80 $[M-H-C_3H_7OH]^-$ in $MS^2$ of base peak ion. LR-$ESI^+$-MS: see details for $[M+H-C_2H_5OH]^+$, $[M+H-C_3H_7OH]^+$, and $[M+H-C_2H_5OH-C_3H_7OH]^+$ isotopic patterns in Fig. S9; m/z 554.94 and 554.96 $[M+H-C_3H_7OH-C_2H_5OH]^+$ in $MS^2$ of base peak ions.

*4.5. Anti-inflammatory Assay*

NO production induced by lipopolysaccharide (LPS) in murine macrophages was evaluated using a previously described method (Choi et al., 2012; Villa et al., 2010). Briefly, RAW 264.7 murine macrophages (ATCC) were cultured 24 h in 96-well plates in Dulbecco's Modified Eagle Medium (Gibco, Carlsbad, CA) supplemented with 10% endotoxin-low fetal bovine serum (HyClone, characterized) ($5x10^4$ cells/185 µL DMEM/well). Controls included LPS (lipopolysaccharide from *Escherichia coli* 026:B6, ≤10,000 EU/mg, Sigma-Aldrich) without compound with 0.75% DMSO and 1% ethanol (positive control), and a 1% ethanol only control

(negative control). The test compounds (10 μL, diluted in 20% ethanol:PBS to yield final concentrations of 32 and 16 μM with 1% ethanol) were added to the appropriate wells. All samples were run in triplicate. Following incubation at 37 °C with 5% $CO_2$ for 1 h, LPS was added to all wells (5 μL, final concentration = 1.0 μg/mL) except for the LPS-free controls. Plates were incubated for an additional 24 h and then Griess reactions were performed using the supernatant fraction (Green et al., 1982). To evaluate for cell viability, an MTT assay was performed with the attached cells. The concentration of nitrite in samples was determined by comparison to a standard curve using regression analysis. The NO concentrations standard curve was prepared based on eight serial dilutions with DMEM of nitrite standard at the range between 0 and100 μM. Cell survival was calculated as a percentage compared to LPS-untreated cells wherein the sample with only 1% EtOH represented 100% survival. Statistical significance analysis was performed by one-way ANOVA followed by Tukey test using GraphPad Prism version 8.0.0 for Windows, GraphPad Software, San Diego, California USA, www.graphpad.com.

**Declaration of competing interest**

The authors confirm that this article content has no conflict of interest.

**Acknowledgements**

This work was supported by the NIH grant CA100851 (W.H.G.), the NIH grant R01 GM107550 (WHG, LG and PCD), the Yangfan Talent Project of Guangdong Province

(201433009) (Y.Z.), the Natural Science Foundation of Guangdong Province (2018A030307046) (Y.Z.), the Free Exploration Project of the Shenzhen Fund for Basic Research (JCYJ20170306165013264) (Y.Z.), the Basic Research Project of Shenzhen Science and Technology Innovation Commission (JCYJ20190813105005619) (Y.Z.), Shenzhen Dapeng New District Industrial Development Fund (KY20180203 & PT201901-05) (Y.Z.), and the Project of Enhancing School with Innovation of Guangdong Ocean University (230420022) (Y.Z.). We also thank Y. Su (UCSD Chemistry and Biochemistry Mass Spectrometry Facility) for the HRESIMS data, A. Mrse (UCSD Chemistry and Biochemistry NMR Facility) for assistance with NMR technical support, and R. Alberstein (UCSD Department of Chemistry) for the help with the CD measurement.

**Supplementary data**

Supplementary data to this article can be found online at: https://doi.org/10.1016/j.phytochem....

**Figures and Legends:**

**Fig**. **1**. The structures of compounds **1**−**8** and two reference compounds **2a** and **2b**.

**Fig. 2**. LC-$MS^2$ based Molecular Network of brominated compounds in the antioxidant sub-fraction 1810E-II

**Fig. 3** The key HMBC (arrows) and COSY (bold bonds) correlations of compounds **1**−**8**

**Fig. 4**. A proposed biogenetic pathway for compound **6**

**Fig**. **5**. The DPPH free radical scavenging activity of compounds compound **1**−**8**. $EC_{50}$ values were

calculated using Prism Graphpad software (n = 3) with variable slopes.

**Fig. 6**. Evaluation of cytotoxicity (line) and inhibition of LPS-induced NO production (bars) by compound **1−8** at 32 μM (no activity was observed at 16 μM). Ethanol (1%) alone served as the negative control, and DMSO (0.75%) was used as the positive control. (n = 3; ****, *** and * represent adjusted P values of <0.0001, 0.0005, and 0.05, respectively). One-way ANOVA followed by Tukey's multiple comparisons test was performed using GraphPad Prism version 8.0.0 for Windows. Amount of NO production calculated from a standard curve (see Supporting Information).

## References


Alfadda, A.A., Sallam, R.M., 2012. Reactive oxygen species in health and disease. J. Biomed. Biotechnol. 2012, 936486.

Choi, H., Mascuch, S.J., Villa, F.A., Byrum, T., Teasdale, M.E., Smith, J.E., Preskitt, L.B., Rowley, D.C., Gerwick, L., Gerwick, W.H., 2012. Honaucins A–C, potent inhibitors of inflammation and bacterial quorum sensing: synthetic derivatives and structure-activity relationships. Chem. Biol. 19, 589–598.

Choi, Y.K., Ye, B.R., Kim, E.A., Kim, J., Kim, M.S., Lee, W.W., Ahn, G.N., Kang, N., Jung, W.K., Heo, S.J., 2018. Bis(3-bromo-4,5-dihydroxybenzyl) ether, a novel bromophenol from the marine red alga *Polysiphonia morrowii* that suppresses LPS-induced inflammatory response by inhibiting ROS-mediated ERK signaling pathway in RAW 264.7 macrophages. Biomed. Pharmacother. 103, 1170–1177.

Dahlgren, E., Enhus, C., Lindqvist, D., Eklund, B., Asplund, L., 2015. Induced production of brominated aromatic compounds in the alga *Ceramium tenuicorne*. Environ. Sci. Pollut. Res. Int. 22, 18107–18114.

Dahlgren, E., Lindqvist, D., Dahlgren, H., Asplund, L., Lehtila, K., 2016. Trophic transfer of naturally produced brominated aromatic compounds in a Baltic Sea food chain. Chemosphere 144, 1597–1604.

Fernando, I.P.S., Nah, J.W., Jeon, Y.J., 2016. Potential anti-inflammatory natural products from marine algae. Environ. Toxicol. Pharmacol. 48, 22–30.

Franceschi, C., Campisi, J., 2014. Chronic inflammation (inflammaging) and its potential contribution to age-associated diseases. J. Gerontol. A Biol. Sci. Med. Sci. 69, S4–S9.

Green, L.C., Wagner, D.A., Glogowski, J., Skipper, P.L., Wishnok, J.S., Tannenbaum, S.R., 1982. Analysis of nitrate, nitrite, and [15N]nitrate in biological fluids. Anal. Biochem. 126, 131–138.

Gribble, G.W., 2015. Biological activity of recently discovered halogenated marine natural products. Mar. Drugs 13, 4044–4136.

Jesus, A., Correia-da-Silva, M., Afonso, C., Pinto, M., Cidade, H., 2019. Isolation and potential biological applications of haloaryl secondary metabolites from macroalgae. Mar. Drugs 17, 73.

Jones, C.G., Martynowycz, M.W., Hattne, J., Fulton, T.J., Stoltz, B.M., Rodriguez, J.A., Nelson, H.M., Gonen, T., 2018. The cryoem method microed as a powerful tool for small molecule structure determination. ACS Cent. Sci. 4, 1587–1592.

Kang, S.Y., Lee, S.Y., Choi, J.H., Jung, J. S., 2014. In vitro anti-bacterial and anti-scuticociliate activities of extract and bromophenols of the marine red alga *Polysiphonia morrowii* with structure-activity relationships. Hanguk Susan Kwahak Hoeji 1, 45–51.

Kurihara, H., Mitani, T., Kawabata, J., Takahashi, K., 1999. Two new bromophenols from the red alga *Odonthalia corymbifera*. J. Nat. Prod. 62, 882–884.

Lee, J.C., Hou, M.F., Huang, H.W., Chang, F.R., Yeh, C.C., Tang, J.Y., Chang, H.W., 2013. Marine algal natural products with anti-oxidative, anti-inflammatory, and anti-cancer properties. Cancer Cell Int. 13, 55.

Leszek, J., Barreto, G.E., Gasiorowski, K., Koutsouraki, E., Avila-Rodrigues, M., Aliev, G., 2016. Inflammatory mechanisms and oxidative stress as key factors responsible for progression of neurodegeneration: role of brain innate immune system. CNS Neurol. Disord.-Drug Targ. 15, 329–336.

Li, K., Li, X.M., Gloer, J.B., Wang, B.G., 2011. Isolation, characterization, and antioxidant activity of bromophenols of the marine red alga *Rhodomela confervoides*. J. Agric. Food Chem. 59, 9916–9921.

Li, K., Li, X.M., Ji, N.Y., Wang, B.G., 2008. Bromophenols from the marine red alga *Polysiphonia urceolata* with DPPH radical scavenging activity. J. Nat. Prod. 71, 28–30.

Lindqvist, D., Dahlgren, E., Asplund, L., 2017. Biosynthesis of hydroxylated polybrominated diphenyl ethers and the correlation with photosynthetic pigments in the red alga *Ceramium tenuicorne*. Phytochemistry 133, 51–58.

Liu, Q.W., Qiao, Q.A., Zhang, T., Sun, L.X., Wang, M.S., 2009. The structure elucidation of a new bromophenol metabolite from *Polysiphonia urceolata* by experimental and DFT theoretical methods. J. Mol. Struct. 929, 1–5.

Liu, Q.W., Tan, C.H., Zhang, T., Zhang, S.J., Han, L.J., Fan, X., Zhu, D.Y., 2006. Urceolatol, a tetracyclic bromobenzaldehyde dimer from *Polysiphonia urceolata*. J. Asian Nat. Prod. Res. 8, 379–383.

Luzzatto-Knaan, T., Garg, N., Wang, M., Glukhov, E., Peng, Y., Ackermann, G., Amir, A., Duggan, B. M., Ryazanov, S., Gerwick, L., Knight, R., Alexandrov, T., Bandeira, N., Gerwick, W. H., Dorrestein, P. C., 2017. Digitizing mass spectrometry data to explore the chemical diversity and distribution of marine cyanobacteria and algae. Elife 6, e24214.

Malmvarn, A., Marsh, G., Kautsky, L., Athanasiadou, M., Bergman, A., Asplund, L., 2005. Hydroxylated and methoxylated brominated diphenyl ethers in the red algae *Ceramium tenuicorne* and blue mussels from the Baltic Sea. Environ. Sci. Technol. 39, 2990–2997.

McBean, G.J., Lopez, M.G., Wallner, F.K., 2017. Redox-based therapeutics in neurodegenerative disease. Brit. J. Pharmacol. 174, 1750–1770.

Meneses, I., 1995. Notes on *Ceramium* (Rhodophyta: Ceramiales) from the Hawaiian Islands. Pacific Sci. 49, 165–174.

Nogueira, C.C., Paixao, I.C., Teixeira, V.L., 2014. Antioxidant activity of natural products isolated from red seaweeds. Nat. Prod. Commun. 9, 1031–1036.

Olsen, E.K., Hansen, E., Isaksson, J., Andersen, J.H., 2013. Cellular antioxidant effect of four bromophenols from the red algae, *Vertebrata lanosa*. Mar. Drugs 11, 2769–2784.

Pedersen, M., Saenger, P., Fries, L., 1974. Simple brominated phenols in red algae. Phytochemistry 13, 2271–2279.

Phillips, D.W., Towers, G.H.N., 1981. Reversed-phase high-performance liquid chromatograhy of red algal bromophenols. J. Chromatogr. A 206, 573–580

Rani, V., Deep, G., Singh, R.K., Palle, K., Yadav, U.C.S., 2016. Oxidative stress and metabolic disorders: Pathogenesis and therapeutic strategies. Life Sci. 148, 183–193.

Reuter, S., Gupta, S.C., Chaturvedi, M.M., Aggarwal, B.B., 2010. Oxidative stress, inflammation, and cancer How are they linked? Free Radical Bio. Med. 49, 1603–1616.

Shi, D.Y., Han, L.J., Fan, X., Xu, F., Liu, Q.W., 2009. Application of two bromophenol compounds in preparing drugs for treating malignant tumor. In: National Intellectual Property Administration, P. C. (Ed.), Faming Zhuanli Shenqing, China.

Siti, H.N., Kamisah, Y., Kamsiah, J., 2015. The role of oxidative stress, antioxidants and vascular inflammation in cardiovascular disease (a review). Vasc. Pharmacol. 71, 40–56.

Spagnuolo, C., Moccia, S., Russo, G.L., 2018. Anti-inflammatory effects of flavonoids in neurodegenerative disorders. Eur. J. Med. Chem. 153, 105–115.

Villa, F.A., Lieske, K., Gerwick, L., 2010. Selective MyD88-dependent pathway inhibition by the cyanobacterial natural product malyngamide F acetate. Eur. J. Pharmacol. 629, 140–146.

Wang, B.G., Gloer, J.B., Ji, N.Y., Zhao, J.C., 2013. Halogenated organic molecules of Rhodomelaceae origin: chemistry and biology. Chem. Rev. 113, 3632–3685.

Wang, M., Carver, J.J., Phelan, V.V., Sanchez, L.M., Garg, N., Peng, Y., Nguyen, D.D., Watrous, J., Kapono, C.A., Luzzatto-Knaan, T., Porto, C., Bouslimani, A., Melnik, A.V., Meehan, M.J., Liu, W.T., Crusemann, M., Boudreau, P.D., Esquenazi, E., Sandoval-Calderon, M., Kersten, R.D., Pace, L.A., Quinn, R.A., Duncan, K.R., Hsu, C.C., Floros, D.J., Gavilan, R.G., Kleigrewe, K., Northen, T., Dutton, R.J., Parrot, D., Carlson, E.E., Aigle, B., Michelsen, C.F., Jelsbak, L., Sohlenkamp, C., Pevzner, P., Edlund, A., McLean, J., Piel, J., Murphy, B.T., Gerwick, L., Liaw, C.C., Yang, Y.L., Humpf, H.U., Maansson, M., Keyzers, R.A., Sims, A.C., Johnson, A.R., Sidebottom, A.M., Sedio, B.E., Klitgaard, A., Larson, C.B., P, C. A. B., Torres-Mendoza, D., Gonzalez, D.J., Silva, D.B., Marques, L.M., Demarque, D.P., Pociute, E., O'Neill, E.C., Briand, E., Helfrich, E.J.N., Granatosky, E.A., Glukhov, E., Ryffel, F., Houson, H., Mohimani, H., Kharbush, J.J., Zeng, Y., Vorholt, J.A., Kurita, K.L., Charusanti, P., McPhail, K.L., Nielsen, K.F., Vuong, L., Elfeki, M., Traxler, M.F., Engene, N., Koyama, N., Vining, O.B., Baric, R., Silva, R.R., Mascuch, S.J., Tomasi, S., Jenkins, S., Macherla, V., Hoffman, T., Agarwal, V., Williams, P.G., Dai, J., Neupane, R., Gurr, J., Rodriguez, A.M.C., Lamsa, A., Zhang, C., Dorrestein, K., Duggan, B.M., Almaliti, J., Allard, P.M., Phapale, P., Nothias, L.F., Alexandrov, T., Litaudon, M., Wolfender, J.L., Kyle, J.E., Metz, T.O., Peryea, T., Nguyen, D.T., VanLeer, D., Shinn, P., Jadhav, A., Muller, R., Waters, K.M., Shi, W., Liu, X., Zhang, L., Knight, R., Jensen, P.R., Palsson, B.O., Pogliano, K., Linington, R.G., Gutierrez, M., Lopes, N.P., Gerwick, W.H., Moore, B.S., Dorrestein, P.C., Bandeira, N., 2016. Sharing and community curation of mass spectrometry data with Global Natural Products Social Molecular Networking. Nat. Biotechnol. 34, 828–837.

Wang, T., Jonsdottir, R., Olafsdottir, G., Kristinsson, H.G., 2014. Antioxidant properties of marine macroalgae. In: Kristinsson, H.G. (Ed.), Antioxidants and Functional Components in Aquatic Foods. John Wiley & Sons, Ltd., pp. 283–317.

Wiemer, D.F., Idler, D.D., Fenical, W., 1991. Vidalols A and B, new anti-inflammatory bromophenols from the Caribbean marine red alga *Vidalia obtusaloba*. Experientia 47, 851–853.

Wu, J.Z., Lin, L., Yu, Y., Wan, X., Yin, X., 2007. Supramolecular isomerism in the hydrogen-bonded network of (5R,10R)-3,8-dihydroxy-5,10-diethoxy-5,10-dihydrochromeno[5,4,3-cde]chromene monohydrate. Struct. Chem. 18, 697–701.

Yang, W.C., Bao, H.Y., Liu, Y.Y., Nie, Y.Y., Yang, J.M., Hong, P.Z., Zhang, Y., 2018. Depsidone derivatives and a cyclopeptide produced by marine fungus *Aspergillus unguis* under chemical induction and by its plasma induced mutant. Molecules 23, 2245–2259.